

Observation of Complex Organic Molecules Containing Peptide-like Bonds Toward Hot Core G358.93–0.03 MM1

Arijit Manna*¹, Sabyasachi Pal¹

¹Department of Physics and Astronomy, Midnapore City College, Paschim Medinipur, West Bengal, India
721129, Email: amanna.astro@gmail.com

Received 2024 April 26; revised 2024 May 31; accepted 2024 June 1; published 2024 July 3

DOI: 10.1088/1674-4527/ad539b

Abstract In star formation regions, the complex organic molecules (COMs) that contain peptide bonds ($-\text{NH}-\text{C}(=\text{O})-$) play a major role in the metabolic process because $-\text{NH}-\text{C}(=\text{O})-$ is connected to amino acids ($\text{R}-\text{CHNH}_2-\text{COOH}$). Over the past few decades, many COMs containing peptide-like bonds have been detected in hot molecular cores (HMCs), hot corinos, and cold molecular clouds, however, their prebiotic chemistry is poorly understood. We present the first detection of the rotational emission lines of formamide (NH_2CHO) and isocyanic acid (HNCO), which contain peptide-like bonds toward the chemically rich HMC G358.93–0.03 MM1, using high-resolution and high-sensitivity Atacama Large Millimeter/submillimeter Array bands 6 and 7. We estimate that the column densities of NH_2CHO and HNCO toward G358.93–0.03 MM1 are $(2.80 \pm 0.29) \times 10^{15} \text{ cm}^{-2}$ and $(1.80 \pm 0.42) \times 10^{16} \text{ cm}^{-2}$ with excitation temperatures of $165 \pm 21 \text{ K}$ and $170 \pm 32 \text{ K}$, respectively. The fractional abundances of NH_2CHO and HNCO toward G358.93–0.03 MM1 are $(9.03 \pm 1.44) \times 10^{-10}$ and $(5.80 \pm 2.09) \times 10^{-9}$. We compare the estimated abundances of NH_2CHO and HNCO with the existing three-phase warm-up chemical model abundance values and notice that the observed and modeled abundances are very close. We conclude that NH_2CHO is produced by the reaction of NH_2 and H_2CO in the gas phase toward G358.93–0.03 MM1. Likewise, HNCO is produced on the surface of grains by the reaction of NH and CO toward G358.93–0.03 MM1. We also find that NH_2CHO and HNCO are chemically linked toward G358.93–0.03 MM1.

Key words: ISM: individual objects (G358.93–0.03) – ISM: abundances – ISM: kinematics and dynamics – stars: formation – astrochemistry

1 INTRODUCTION

In complex organic molecules (hereafter COMs), the peptide bond [–NH–C(=O)–] links two amino acids to produce proteins. So, those COMs with peptide bonds provide information regarding the origin of life in the universe. In the interstellar medium (ISM), formamide (NH₂CHO), cyanamide (NH₂CN), isocyanic acid (HNCO), and acetamide (CH₃CONH₂) are COMs containing peptide-like bonds. NH₂CHO has an amide-amide bond (–N–C(=O)–), which is crucial for the synthesis of proteins. NH₂CHO contains carbon (C), hydrogen (H), oxygen (O), and nitrogen (N), which are important for biological systems. NH₂CHO also acts as a prebiotic precursor of genetic and metabolic materials (Saladino et al. 2012). The dipole moment of NH₂CHO is $\mu_a = 3.61$ Debye and $\mu_b = 0.852$ (Kurland & Wilson 1957). The emission lines of NH₂CHO were first detected in high-mass star-formation regions Sgr B2 and Orion KL (Rubin et al. 1971). The evidence of NH₂CHO was also found in several high- and low-mass star-formation regions (Bisschop et al. 2007; Adande et al. 2013; Kahane et al. 2013; López-Sepulcre et al. 2015; Manna et al. 2024a), extragalactic sources (Muller et al. 2013), comets (Bockelée-Morvan et al. 2000; Biver et al. 2014; Goesmann et al. 2015), and shocked regions (Yamaguchi et al. 2012; Mendoza et al. 2014).

In ISM, isocyanic acid (HNCO) is the simplest organic molecule, consisting of four biogenic elements, C, H, O, and N, all of which are present in living bodies. HNCO also acts as a precursor of several prebiotic COMs, including those molecules linked with astrochemical and astrobiological interest, such as amino acids, nucleobases, and sugars (Gorai et al. 2020; Fedoseev et al. 2020). Laboratory experiments suggested that CH₄ and HNCO can produce peptide-bonded molecules in the solid state (Ligterink et al. 2018). HNCO is a prolate asymmetric top molecule, and its rotational levels exhibit hyperfine splitting owing to the nuclear spin of nitrogen (Niedenhoff et al. 1995; Lapinov et al. 2007). The dipole moment of HNCO is $\mu_a = 1.60$ Debye and $\mu_b = 1.35$ Debye (Kukolich et al. 1971). The evidence of HNCO was first found towards Sgr B2 (Snyder et al. 1972; Churchwell et al. 1986; Kuan & Snyder 1996). Additionally, evidence of HNCO has also been found towards hot cores and hot corinos (Blake et al. 1987; van Dishoeck et al. 1995; MacDonald et al. 1996; Bisschop et al. 2008; Gorai et al. 2020; Canelo et al. 2021), galactic molecular clouds (Jackson et al. 1984; Zinchenko et al. 2000), and translucent clouds (Turner et al. 1999). Although there were many chemical modelling works to investigate the evolution of NH₂CHO and HNCO, the formation pathways of both molecules remain unclear (Gorai et al. 2020).

The most chemically rich objects in the ISM are the hot molecular cores (hereafter HMCs) (Bisschop et al. 2007; Belloche et al. 2013; Manna & Pal 2022a,b; Manna et al. 2023). HMCs represent the early phases of high-mass star-forming regions. The typical masses of HMCs are $\geq 100 M_{\odot}$, which indicates that HMCs

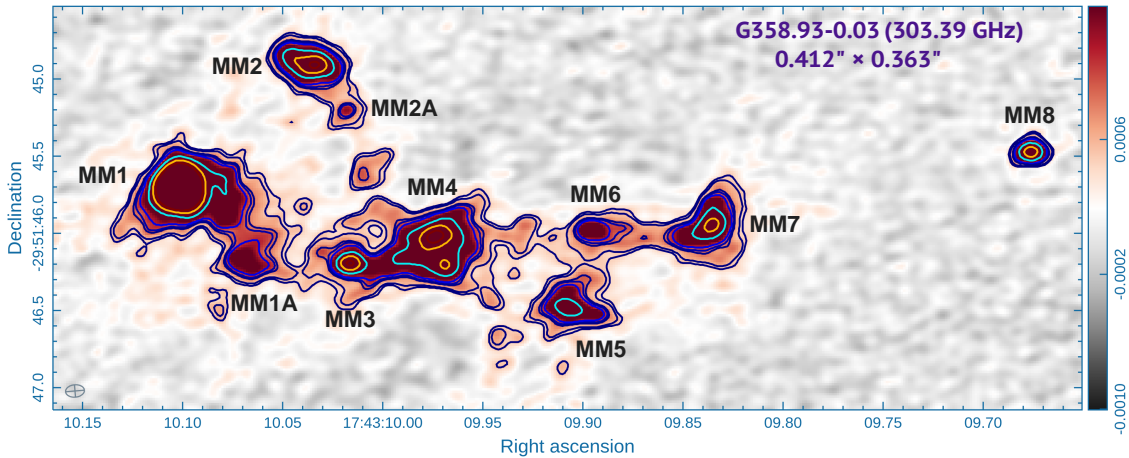


Fig. 1 Millimeter wavelength continuum emission image of massive star-formation region G358.93–0.03 at a frequency of 303.39 GHz. The synthesized beam size of the image is $0.41'' \times 0.36''$. The contour levels start at 2.5σ and increase by a factor of $\sqrt{2}$.

are reservoirs of several types of COMs, including precursors of $\text{NH}_2\text{CH}_2\text{COOH}$ (van Dishoeck & Blake 1998). Our current idea regarding high-mass star formation regions is incomplete due to a lack of a sufficient number of observations of this kind of source. Recent observational studies indicate the evolution of high-mass star-forming regions as follows: infrared dark clouds (IRDCs) \rightarrow HMCs \rightarrow hyper/ultra-compact H II regions \rightarrow H II regions, which are surrounded by ionized high-mass stars (Beuther et al. 2007). The middle stages between the IRDCs and ultracompact HII regions are known as the HMCs. Owing to the lack of UV photons, the temperatures of the central protostars in the HMCs rise because of the increase in the temperatures of the dust and gaseous material. In ISM, HMCs have a high gas density ($n_{\text{H}_2} \geq 10^6 \text{ cm}^{-3}$), a warm temperature ($\geq 100 \text{ K}$), and a compact and small source size ($\leq 0.1 \text{ pc}$) (van Dishoeck & Blake 1998; Williams & Viti 2014). Previous molecular line surveys at millimeter and sub-millimeter wavelengths show that several types of COMs like CH_3OH , CH_3OCHO , CH_3OCH_3 , CH_3CN , and $\text{C}_2\text{H}_5\text{CN}$ are frequently found in different HMCs because of the high temperature and evaporation of H_2O and organic ice mantles (Herbst & van Dishoeck (2009), and references therein).

G358.93–0.03 (RA: $17^{\text{h}}43^{\text{m}}10^{\text{s}}.02$, Dec: $-29^{\circ}51'45.8''$) is the massive star-forming region that was located $6.75^{+0.37}_{-0.68}$ kpc from Earth (Reid et al. 2014; Brogan et al. 2019). There are eight sub-millimeter continuum sources in G3589.93–0.03, which have been designated from G3589.93–0.03 MM1 to G3589.93–0.03 MM8 in decreasing right ascension (R.A) (Brogan et al. 2019). The luminosity and mass of G358.93–0.03 are $\sim 7.7 \times 10^3 L_{\odot}$ and $167 \pm 12 M_{\odot}$, respectively (Brogan et al. 2019). Two of the eight sources, G358.93–0.03 MM1 (hereafter MM1) and G358.93–0.03 MM3 (hereafter MM3), have been confirmed as having line-rich hot molecular cores (Brogan et al. 2019; Bayandina et al. 2022). Earlier, maser lines of CH_3OH , $^{13}\text{CH}_3\text{OH}$, HNCO , and HDO were detected towards MM1 using the ALMA, TMRT, and VLA

radio telescopes (Brogan et al. 2019; Chen et al. 2020). Except for the maser lines, Brogan et al. (2019) also detected the emission lines of CH_3CN from MM1 and MM3, but they do not estimate the abundance of this molecule. The emission lines of NH_2CN , the simplest sugar-like molecule CH_2OHCHO , and the antifreeze molecule $(\text{CH}_2\text{OH})_2$, and possible $\text{NH}_2\text{CH}_2\text{COOH}$ precursor molecule CH_3NH_2 were also detected towards MM1 using the ALMA bands 6 and 7 (Manna & Pal 2023; Manna et al. 2023, 2024b; Manna & Pal 2024). The detection of the above-mentioned molecules indicates that the MM1 is an ideal candidate for studying the emission lines of different types of complex biomolecules, including biologically relevant molecules.

In this paper, we report the first detection of the emission lines of NH_2CHO and HNCO towards the hot molecular core MM1 with the ALMA. The gas temperature and column density of NH_2CHO and HNCO were estimated using the local thermodynamic equilibrium (LTE) model. We also address the probable formation pathways of NH_2CHO and HNCO towards MM1. The observations and data analysis are shown in section 2. The results of the emission line detection of NH_2CHO and HNCO are shown in Section 3. The discussion and conclusions are presented in Sections 4 and 5.

2 OBSERVATION AND DATA REDUCTIONS

We used openly available raw data of the massive star-forming region G358.93–0.03, observed with the Atacama Large Millimeter/Submillimeter Array (ALMA) 12-m arrays with bands 6 and 7 (which span the frequency ranges of 290.51–306.01 GHz and 225.44–242.06 GHz) (PI: Crystal Brogan). The band 6 observation was performed in four spectral windows with frequency ranges of 225.44–226.38 GHz, 229.48–229.72 GHz, 240.26–241.20 GHz, and 241.12–242.06 GHz. Similarly, the band 7 observation was performed in four spectral windows with frequency ranges of 290.51–292.39 GHz, 292.49–294.37 GHz, 302.62–304.49 GHz, and 304.14–306.01 GHz. The ALMA bands 6 and 7 observations were conducted on April 16, 2019 and November 11, 2019, with on-source integration times of 3265.92 sec and 756.0 sec. The star-formation region G358.93–0.03’s phase centre was $(\alpha, \delta)_{\text{J2000}} = 17:43:10.000, -29:51:46.000$. To observe G358.93–0.03 in ALMA band 6, 45 antennas were set up with a minimum baseline of 15.1 m and a maximum baseline of 740.4 m. To observe G358.93–0.03 for ALMA band 7, 47 antennas were set up with a minimum baseline of 14 m and a maximum baseline of 2517 m. The bandpass and flux calibrators for bands 6 and 7 during the observations were J1924–2914 and J1550+0527, respectively, whereas the phase calibrator for bands 6 and 7 was J1744–3116.

We employed the Common Astronomy Software Application (CASA 5.4.1) with an ALMA data analysis pipeline for data reduction and imaging (McMullin et al. 2007). We utilized the Perley-Butler 2017 flux calibrator model with the SETJY task for flux calibration (Perley & Butler 2017). After flagging the bad antenna data, we subsequently constructed the flux and bandpass calibration using pipeline tasks

HIFA_BANDPASSFLAG and HIFA_FLAGDATA. We separated the target data with all available rest frequencies using the CASA task MSTRANSFORM after gain calibration. Utilizing the CASA task TCLEAN with line-free channels, we constructed a continuum emission image of G358.93–0.03. The continuum emission image of G358.93–0.03 at a frequency of 303.39 GHz is shown in Figure 1. Utilizing these data, Manna et al. (2023) recently investigated in detail the dust continuum emissions from G358.93–0.03 (see Figure 1 in Manna et al. (2023)). In addition to eight sources, Manna et al. (2023) also discovered two additional sources associated with MM1 and MM2, which are referred to as MM1A and MM2A. Thus, in this study, we did not address the continuum emission characteristics of G358.93–0.03. Next, we employ the UVCONTSUB task to remove the continuum emission from the UV plane of the calibrated data. After that, to produce spectral data cubes of G358.93–0.03, we used the CASA task TCLEAN with the SPECMODE = CUBE parameter and Briggs weighting at a robust value of 0.5. Finally, we corrected the primary beam pattern in continuum images and spectral data cubes using the IMPBCOR task.

3 RESULT

3.1 Molecular lines in G358.93–0.03

In the spectral data cubes of G358.93–0.03, we observed molecular line emissions from hot cores MM1 and MM3. We did not find any molecular line emissions from other sources in G358.93–0.03. The synthesized beam sizes of the spectral data cubes of G358.93–0.03 at ALMA band 6 were $0.55'' \times 0.45''$, $0.53'' \times 0.46''$, $0.52'' \times 0.42''$, and $0.51'' \times 0.42''$. Similarly, the synthesized beam sizes of the spectral data cubes at ALMA band 7 were $0.42'' \times 0.36''$, $0.42'' \times 0.37''$, $0.41'' \times 0.36''$, and $0.41'' \times 0.35''$, respectively. The molecular spectra were extracted by drawing a $0.90''$ diameter circular region over the MM1 and MM3, which is greater than the line emitting regions of both hot cores. The pointing centre of MM1 is α (J2000) = $17^h 43^m 10^s.101$, δ (J2000) = $-29^\circ 51' 45''.693$. Similarly, the pointing centre of MM3 is α (J2000) = $17^h 43^m 10^s.0144$, δ (J2000) = $-29^\circ 51' 46''.193$. Recently, Manna et al. (2023) used this band 7 data, and they claimed that MM1 is more chemically rich than MM3. In the band 7 molecular spectra of MM1, Manna et al. (2023) noticed an inverse P-cygni profile in the emission lines of CH₃OH. That indicates MM1 is undergoing an infall. Manna et al. (2023) did not see any inverse P-cygni profile in the emission lines of CH₃OH towards MM3. The velocities of the spectra (V_{LSR}) of MM1 and MM3 are -16.5 km s⁻¹ and -18.2 km s⁻¹, respectively, (Manna et al. 2023; Manna & Pal 2024). From the chemically rich spectra, we focused only on studying the emission lines of COMs that contain peptide-like bonds, which are discussed in the following sections.

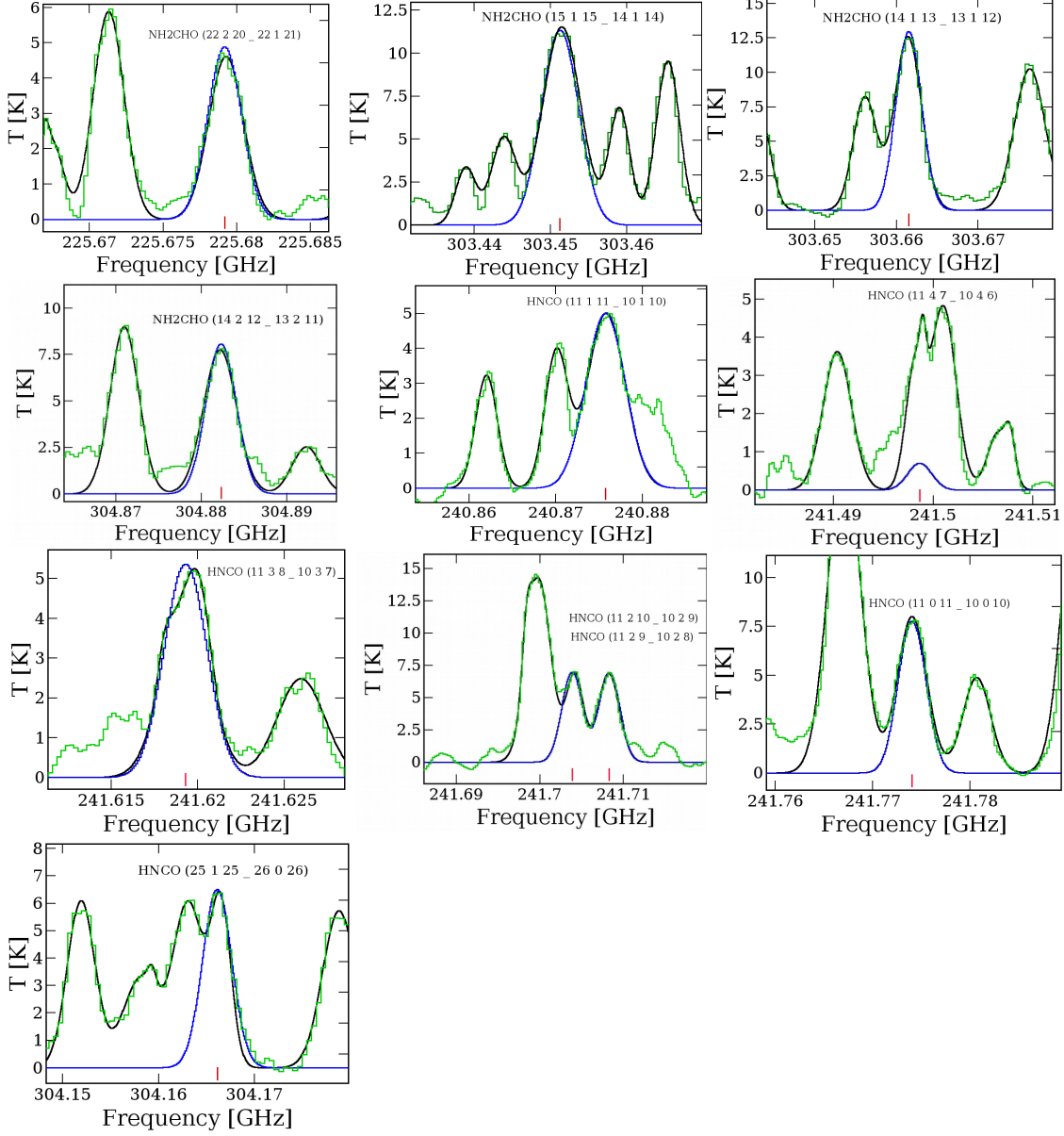


Fig. 2 Emission lines of NH_2CHO and HNC0 towards the MM1. The green lines represent the observed molecular spectra of MM1. The fitted blue spectra indicate the LTE-modelled spectra of NH_2CHO and HNC0 . The fitted black spectra indicate the LTE-modelled spectra of other nearby molecules to understand the blended effect. The velocity of the spectra is -16.50 km s^{-1} .

3.2 Rotational emission lines NH_2CHO towards MM1

We employed the local thermodynamic equilibrium (LTE) model with the Cologne Database for Molecular Spectroscopy (CDMS) and Jet Population Laboratory (JPL) molecular databases to find the rotational emission lines of NH_2CHO from the chemically rich molecular spectra of MM1 (Müller et al. 2005; Pickett et al. 1988). For fitting the LTE spectral model over the observed emission lines of NH_2CHO , we employed

Table 1 Molecular line properties of NH₂CHO and HNCO towards the MM1.

Molecule	Frequency (GHz)	Transition ($J'_{K'_a K'_c} - J''_{K''_a K''_c}$)	E_u (K)	A_{ij} (s ⁻¹)	g_{up}	$S\mu^2$ (Debye ²)	FWHM (km s ⁻¹)	$\int T_{mb} dV$ (K km s ⁻¹)	Optical depth (τ)	Remarks
NH ₂ CHO	225.679	22(2,20)–22(1,21)	275.80	3.20×10^{-5}	45	10.762	3.55 ± 0.82	13.57 ± 0.43	1.37×10^{-1}	Non blended
	303.451	15(1,15)–14(1,14)	120.01	2.05×10^{-3}	93	585.30	3.58 ± 0.29	44.61 ± 0.96	2.04×10^{-1}	Non blended
	303.661	14(1,13)–13(1,12)	113.00	2.04×10^{-3}	87	545.30	3.56 ± 0.37	42.71 ± 0.34	1.99×10^{-1}	Non blended
	304.882	14(2,12)–13(2,11)	120.54	2.04×10^{-3}	87	538.17	3.55 ± 0.44	27.44 ± 0.52	1.88×10^{-1}	Non blended
HNCO	240.875	11(1,11)–10(1,10)	112.64	1.90×10^{-4}	23	26.922	3.55 ± 0.62	20.56 ± 0.82	1.98×10^{-1}	Non blended
	241.498*	11(4,7)–10(4,6)	720.30	1.40×10^{-4}	23	19.679	–	–	1.04×10^{-2}	Blended with CHDCO
	241.619*	11(3,8)–10(3,7)	444.56	1.63×10^{-4}	23	22.877	3.58 ± 0.59	18.45 ± 0.34	8.55×10^{-2}	Non blended
	241.703*	11(2,10)–10(2,9)	239.89	1.81×10^{-4}	23	25.357	3.49 ± 0.21	15.28 ± 0.22	2.27×10^{-1}	Non blended
	241.708*	11(2,9)–10(2,8)	239.89	1.81×10^{-4}	23	25.356	3.48 ± 0.35	20.67 ± 0.61	2.37×10^{-1}	Non blended
	241.774	11(0,11)–10(0,10)	69.62	1.96×10^{-4}	23	27.458	3.52 ± 0.69	29.54 ± 0.87	5.69×10^{-1}	Non blended
	304.166	25(1,25)–26(0,26)	384.78	1.50×10^{-4}	51	23.34	3.55 ± 0.92	15.81 ± 0.21	1.13×10^{-1}	Non blended

*–There are two transitions less than 100 kHz. We showed only the first transition.

the Markov Chain Monte Carlo (MCMC)¹ algorithm in the CASSIS software package (Vastel et al. 2015). The gas density of the inner region of MM1 is 2×10^7 cm⁻³, indicating that the LTE assumptions are true for this source (Stecklum et al. 2021). Through analysing the molecular spectra using the LTE model, we have detected four rotational emission lines of the complex N- and O-bearing molecule NH₂CHO towards MM1. The upper state energies of the detected emission lines of NH₂CHO varied between 113 K and 275.80 K. After detecting the emission lines of NH₂CHO, we obtained the molecular transitions, upper state energy (E_u) in K, Einstein coefficients (A_{ij}) in s⁻¹, line intensity ($S\mu^2$) in Debye², full-width half maximum (FWHM) in km s⁻¹, optical depth (τ), and integrated intensities ($\int T_{mb} dV$) in K km s⁻¹. The LTE fitting spectral lines of NH₂CHO are shown in Figure 2 and the corresponding spectral parameters are listed in Table 1. Except for NH₂CHO, we also fitted the rest of the 250 molecular transitions, which were taken from CDMS and JPL molecular databases, across the observed spectra of MM1 to better understand the blending effect. After spectral analysis, we noticed that all detected lines of NH₂CHO are non-blended, and all transition lines exhibit $\geq 4 \sigma$ statistical significance. The best-fit column density of NH₂CHO is $(2.80 \pm 0.29) \times 10^{15}$ cm⁻² with an excitation temperature of 165 ± 21 K, which was estimated based on LTE modelling. The estimated excitation temperature of NH₂CHO suggests this molecule originates from the warm inner region of MM1 because the gas temperature of the warm inner region of the hot molecular cores is above 100 K (van Dishoeck & Blake 1998; Williams & Viti 2014). The abundance of NH₂CHO towards MM1 with respect to molecular H₂ is $(9.03 \pm 1.44) \times 10^{-10}$, where the column density of molecular H₂ towards MM1 is $(3.10 \pm 0.2) \times 10^{24}$ cm⁻² (Manna et al. 2023).

¹ https://cassis.irap.omp.eu/docs/CassisScriptingDoc/computation/mcmc_method.html#mcmc-method

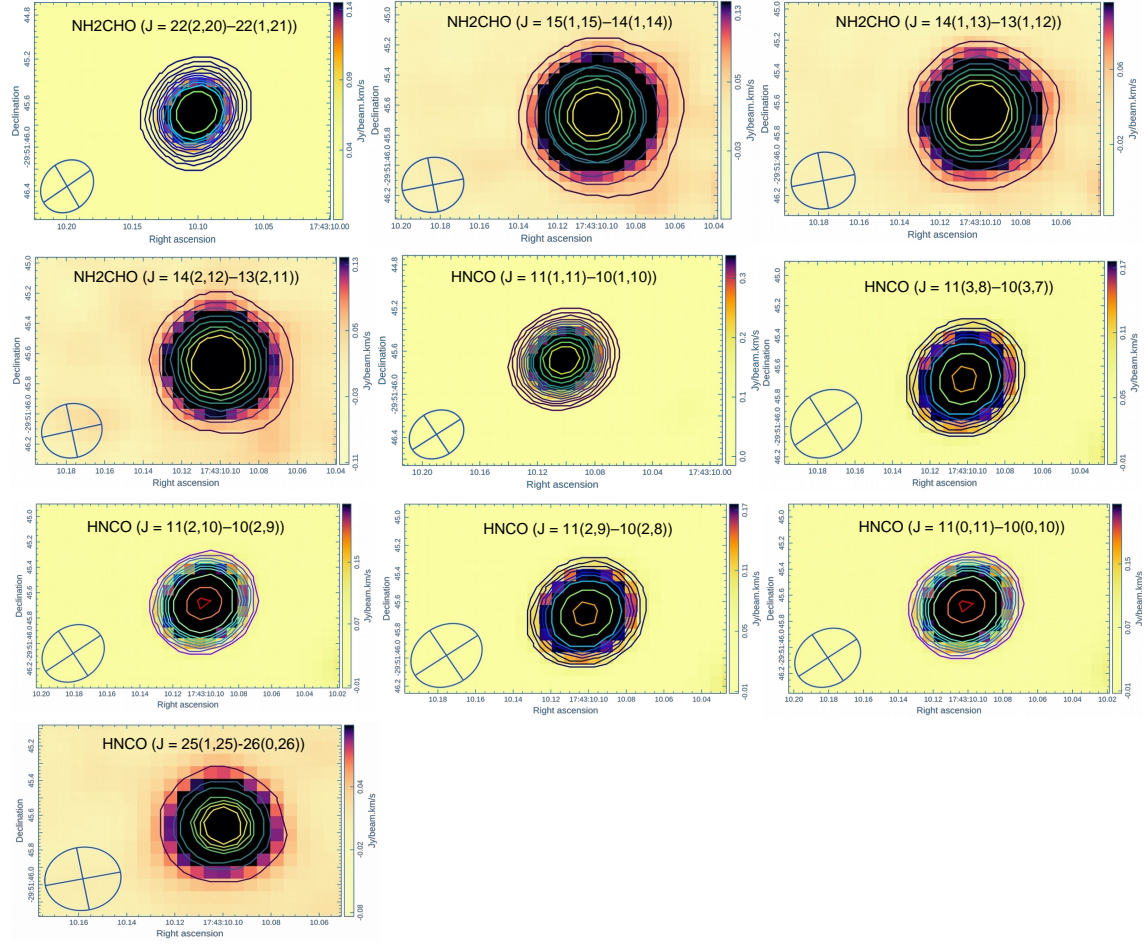


Fig. 3 Emission maps of detected non-blended transitions of NH_2CHO and HNCO towards the MM1. The contours are the $988 \mu\text{m}$ continuum emission map of G358.93–0.03. The contour levels start at 3σ .

3.3 Rotational emission lines of HNCO towards MM1

Using the LTE-modelled spectra, we detected seven rotational emission lines of HNCO towards MM1 using the ALMA bands 6 and 7. The upper-state energies (E_u) of the identified rotational emission lines of HNCO vary between 69.62 K and 720.30 K. After spectral analysis, we noticed that the emission line of HNCO at a frequency of 241.498 GHz ($J = 11(4,7)–10(4,6)$) is blended with CHDCO . All other detected transitions are non-blended. The non-blended emission lines of HNCO exhibited $\geq 4.5 \sigma$ statistical significance. The resultant LTE-fitted spectral line and spectra line parameters of HNCO are shown in Figure 2 and Table 1. The best-fit column density of HNCO is $(1.80 \pm 0.42) \times 10^{16} \text{ cm}^{-2}$ with an excitation temperature of 170 ± 32 K, which was estimated based on LTE modelling. The abundance of HNCO with respect to molecular H_2 towards the MM1 is $(5.80 \pm 2.09) \times 10^{-9}$, where the column density of molecular H_2 towards the MM1 is $(3.10 \pm 0.2) \times 10^{24} \text{ cm}^{-2}$ (Manna et al. 2023).

3.4 Searching the emission lines of NH₂CHO and HNCO towards MM3

After the detection of the rotational emission lines of NH₂CHO and HNCO towards MM1, we used the LTE-modelled spectra to search for these molecules towards MM3. However, we were unable to find the emission lines of those molecules towards MM3. As per the LTE analysis, the upper limit column densities of NH₂CHO and HNCO towards MM3 are $\leq(2.05\pm 0.85)\times 10^{13}$ cm⁻² and $\leq(8.12\pm 1.26)\times 10^{14}$ cm⁻², respectively. The upper limit of the abundances of NH₂CHO and HNCO towards MM3 are $\leq(5.84\pm 1.26)\times 10^{-11}$ and $\leq(2.31\pm 1.27)\times 10^{-9}$, where the column density of molecular H₂ towards the MM3 is $(3.51\pm 0.7)\times 10^{23}$ cm⁻² (Manna et al. 2023).

3.5 Spatial distribution of NH₂CHO and HNCO towards MM1

After detection of the emission lines of NH₂CHO and HNCO towards MM1, we produced the integrated emission maps of the non-blended emission lines of those molecules by integrating the spectral data cubes using the channel ranges with the help of CASA task `IMMOMENTS`. The emission maps of NH₂CHO and HNCO towards MM1 are presented in Figure 3. The emission maps of NH₂CHO and HNCO are overlaid with a 988 μ m continuum emission image of G358.93–0.03. The dust continuum image of G358.93–0.03 is taken from Manna et al. (2023). From the integrated emission maps, we observed that NH₂CHO and HNCO arose from the warm-inner regions of MM1. Since the excitation temperature of NH₂CHO and HNCO towards MM1 is 165 ± 21 K and 170 ± 32 K, which indicates both molecules may exist in the same region of MM1. So, there is a high chance of a chemical link between NH₂CHO and HNCO towards MM1. We estimate the size of the emitting regions of NH₂CHO and HNCO by fitting the 2D Gaussians over the emission maps of NH₂CHO and HNCO using the `IMFIT` task. The sizes of the emitting regions of NH₂CHO and HNCO corresponding to the non-blended transition lines are shown in Table 2. We observed that the emitting regions of NH₂CHO and HNCO are similar or marginally larger than the beam sizes of the emission maps. This suggests that the emission maps of NH₂CHO and HNCO are not spatially resolved towards MM1. Therefore, we could not determine the chemical morphologies of NH₂CHO and HNCO from the integrated emission maps. Higher spatial and angular resolution observations are needed to learn the spatial distribution of NH₂CHO and HNCO towards MM1.

3.6 Searching of other peptide bonds molecules towards MM1

After the detection of the rotational emission lines of NH₂CHO and HNCO towards MM1, we also search the rotational emission lines of other COMs that have peptide bonds, such as HOCH₂C(O)NH₂, CH₃NCO, CH₃NHCHO, NH₂C(O)CN, CH₃CH₂NCO, CH₃C(O)NH₂, and NH₂C(O)NH₂ using the LTE modelled spectra. During the spectral analysis, we observed that all the above-mentioned molecules are

Table 2 Emitting regions of NH₂CHO and HNCO towards the MM1.

Molecule	Frequency GHz	Transition ($J'_{K'_a K'_c} - J''_{K''_a K''_c}$)	E_{up} (K)	Emitting region ($''$)
NH ₂ CHO	225.679	22(2,20)–22(1,21)	275.80	0.42
	303.451	15(1,15)–14(1,14)	120.01	0.43
	303.661	14(1,13)–13(1,12)	113.00	0.42
	304.882	14(2,12)–13(2,11)	120.54	0.43
HNCO	240.875	11(1,11)–10(1,10)	112.64	0.42
	241.619*	11(3,8)–10(3,7)	444.56	0.42
	241.703*	11(2,10)–10(2,9)	239.89	0.43
	241.708*	11(2,9)–10(2,8)	239.89	0.43
	241.774	11(0,11)–10(0,10)	69.62	0.43
	304.166	25(1,25)–26(0,26)	384.78	0.44

*–There are two transitions within less than 100 kHz. We show only the first transition.

blended with other molecular transitions. So, there is a very low chance of identifying these molecules. The upper-limit column densities of peptide bond molecules HOCH₂C(O)NH₂, CH₃NCO, CH₃NHCHO, NH₂C(O)CN, CH₃CH₂NCO, CH₃C(O)NH₂, and NH₂C(O)NH₂ are $\leq 3.56 \times 10^{14} \text{ cm}^{-2}$, $\leq 8.26 \times 10^{14} \text{ cm}^{-2}$, $\leq 5.20 \times 10^{13} \text{ cm}^{-2}$, $\leq 2.96 \times 10^{13} \text{ cm}^{-2}$, $\leq 9.62 \times 10^{13} \text{ cm}^{-2}$, $\leq 1.16 \times 10^{14} \text{ cm}^{-2}$, and $\leq 9.28 \times 10^{12} \text{ cm}^{-2}$, respectively.

4 DISCUSSION

4.1 Comparison of the abundances of NH₂CHO and HNCO towards MM1 and other sources

To understand the distribution of NH₂CHO and HNCO in the ISM, we compare the fractional abundance of those molecules towards MM1 and other hot molecular cores such as G10.47+0.03, G31.41+0.31, Orion KL, Sgr B2, and hot corino object IRAS 16293–2422 B. This comparison is presented in Table 3. After comparison, we noticed that the fractional abundance of NH₂CHO towards MM1 is nearly similar to Sgr B2 and IRAS 16293–2422 B. The fractional abundance of NH₂CHO towards MM1 is one order of magnitude lower than the G31.41+0.31, G10.47+0.03, and Orion KL. Similarly, the fractional abundance of HNCO towards MM1 is similar to that of Orion KL and Sgr B2. The fractional abundance of HNCO is one order of magnitude lower than that of G10.47+0.03 and G31.41+0.31. Furthermore, we notice that the fractional abundance of HNCO towards MM1 is two orders of magnitude larger than that of IRAS 16293–2422 B. Based on that comparison, we identify that G31.41+0.31 and G10.47+0.03 are the most abundant NH₂CHO and HNCO sources in the ISM. The low abundances of NH₂CHO and HNCO towards MM1 indicate that the detection probabilities of other peptide bond COMs are very low in these sources.

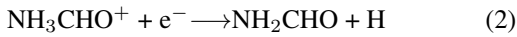
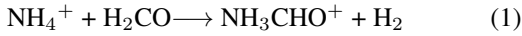
Table 3 Comparison of the abundances of NH₂CHO and HNCO towards the MM1 and other sources.

Molecule	MM1 ^a	G10.47+0.03 ^b	G31.41+0.31 ^c	Orion KL ^d	Sgr B2 ^e	IRAS 16293–2422 B ^f
NH ₂ CHO	$(9.03 \pm 1.44) \times 10^{-10}$	2.87×10^{-9}	$(5.4 \pm 1.5) \times 10^{-9}$	5.80×10^{-9}	1.3×10^{-10}	1.05×10^{-10}
HNCO	$(5.80 \pm 2.09) \times 10^{-9}$	1.02×10^{-8}	$(1.1 \pm 0.3) \times 10^{-8}$	4.08×10^{-9}	7.20×10^{-9}	$(1.8 \pm 0.4) \times 10^{-11}$

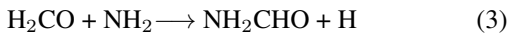
Notes: a: Our work, b: [Gorai et al. \(2020\)](#), c: [Colzi et al. \(2021\)](#), d: [Kahane et al. \(2013\)](#), [Tercero et al. \(2010\)](#), e: [Halfen et al. \(2011\)](#), [Adande et al. \(2010\)](#), f: [Kahane et al. \(2013\)](#), [Hernández-Gómez et al. \(2019\)](#)

4.2 Possible formation mechanism of NH₂CHO and HNCO towards MM1

The formation mechanism(s) of NH₂CHO in ISM is still debatable in the astrochemistry community. We observed that only a few reactions have been proposed to understand the formation pathways of NH₂CHO in both the grain surface and the gas phase. Previously, [Quan & Herbst \(2007\)](#) claimed that the NH₂CHO created via the ion-molecule reaction and subsequent electron recombination reaction between NH₄⁺ and H₂CO:



Subsequently, [Garrod et al. \(2008\)](#) claimed that the rates of reactions 1 and 2 are unknown. In particular, [Garrod et al. \(2008\)](#) proposed the following radical-neutral reaction in the gas phase:

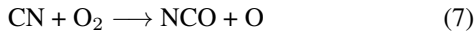


However, [Redondo et al. \(2014\)](#) showed that the net activation barrier energy of this reaction is above 1000 K. Earlier, [Garrod \(2013\)](#) and [Gorai et al. \(2020\)](#) showed that reaction 3 is responsible for the formation of NH₂CHO towards hot molecular cores and hot corions. Previously [Coutens et al. \(2016\)](#) showed that NH₂CHO was formed via the reaction between H₂CO and NH₂ (reaction 3) in the gas phase towards the hot corino IRAS 16293–2422 B. Similarly, reaction 3 is also responsible for the formation of NH₂CHO in the shock region L1157–B1, hot cores Sgr B2 (N), G10.47+0.03, Orion KL, G31.41+0.31, and the high-mass protostar IRAS 18089–1732 ([Halfen et al. 2011](#); [Kahane et al. 2013](#); [Codella et al. 2017](#); [Gorai et al. 2020](#); [Colzi et al. 2021](#); [Manna et al. 2024a](#)).

Previous studies have proposed that the emission lines of HNCO originate from the high-density warm-inner regions of hot cores and hot corinos. Therefore, HNCO may play an important role as a tracer for dense gases in hot molecular cores ([Jackson et al. 1984](#)). Previously, [Iglesias \(1977\)](#) claimed that the HNCO produced in the gas phase via the ion-neutral reaction towards Sgr B2:



Previously, [Turner \(2000\)](#) suggested another neutral-neutral reaction to create HNCO:



Reaction 8 has an activation barrier. Previously, [Garrod et al. \(2008\)](#) showed that the HNCO also formed on the grain surface via the thermal reaction:



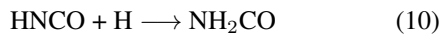
[Garrod et al. \(2008\)](#) claimed that reaction 9 has no activation barrier and that the molecule is released in the gas phase via desorption. Earlier, [Garrod \(2013\)](#) and [Gorai et al. \(2020\)](#) show that reaction 9 is the most efficient reaction for the formation of HNCO towards the hot molecular cores.

Previously, [Gorai et al. \(2020\)](#) computed a three-phase (gas + grain + ice mantle) warm-up chemical model to understand the possible formation mechanisms of NH_2CHO and HNCO. During chemical modelling, they assumed the free-fall collapse of a cloud (Phase I), which was followed by the warm-up phase. In phase I, the density of the gas rapidly increased from 10^3 cm^{-3} to $1 \times 10^7 \text{ cm}^{-3}$ and the dust temperature was constant at 10 K. In phase II (the warm-up stage), the dust temperature was increased from 10 K to 400 K, and the density of the gas was constant at $1 \times 10^7 \text{ cm}^{-3}$. At this stage, the gas and dust in the hot core were well coupled. During chemical modelling, [Gorai et al. \(2020\)](#) used the radical-neutral reaction between H_2CO and NH_2 (reaction 3) and the reaction between NH and CO (reaction 9) for the formation of NH_2CHO and HNCO in the gas phase and grain surface, respectively. Previously, [Garrod \(2013\)](#) also showed that reactions 3 and 9 are the most efficient for the formation of NH_2CHO and HNCO in the gas phase and grain surface towards hot molecular cores. In the warm-up stage, [Gorai et al. \(2020\)](#) estimated the modelled abundances of NH_2CHO and HNCO towards hot molecular cores to be 8.27×10^{-10} and 4.8×10^{-9} , respectively.

To understand the possible formation mechanism of NH_2CHO and HNCO towards MM1, we compared our derived abundance of NH_2CHO and HNCO with the modelled abundance of [Gorai et al. \(2020\)](#). This comparison is reasonable because the gas density and temperature of this source are $2 \times 10^7 \text{ cm}^{-3}$ and 150 K, respectively ([Chen et al. 2020](#); [Stecklum et al. 2021](#)). Therefore, the three-phase warm-up chemical model of [Gorai et al. \(2020\)](#) is efficient for understanding the formation pathways of NH_2CHO and HNCO towards the MM1. [Gorai et al. \(2020\)](#) derived the modelled abundance of NH_2CHO and HNCO to be 8.27×10^{-10} and 4.8×10^{-9} , respectively. The observed fractional abundances of NH_2CHO and HNCO towards MM1 are $(9.03 \pm 1.44) \times 10^{-10}$ and $(5.80 \pm 2.09) \times 10^{-9}$, which are nearly similar to the modelled abundance results in [Gorai et al. \(2020\)](#). This result indicates that NH_2CHO is produced by the reaction of NH_2 and H_2CO in the gas phase towards MM1. Similarly, HNCO is created by the reaction of NH and CO on the surface of the grains of the MM1.

4.3 Chemical link between NH_2CHO and HNCO

Several studies have shown that NH_2CHO and HNCO are chemically connected. Earlier, [Garrod et al. \(2008\)](#), [Haupa et al. \(2019\)](#), and [Gorai et al. \(2020\)](#) claimed that the subsequently hydrogenation of HNCO creates NH_2CHO in the grain surface:



In another way, [López-Sepulcre et al. \(2015\)](#) demonstrated the molecular correlation between the abundance of HNCO and NH_2CHO towards the high-mass star-formation regions. From the molecular correlation plot, [López-Sepulcre et al. \(2015\)](#) found a positive correlation between the abundances of NH_2CHO and HNCO , and they found a correlation equation $X(\text{NH}_2\text{CHO}) = 0.04X(\text{HNCO})^{0.93}$ (see Figures 2 and 3 in [López-Sepulcre et al. \(2015\)](#)). According to the molecular correlation equation of [López-Sepulcre et al. \(2015\)](#), we found that the abundance of NH_2CHO is $(8.75 \pm 1.98) \times 10^{-10}$, which is very similar to our observed abundance of NH_2CHO towards MM1. This result indicates that HNCO and NH_2CHO are chemically connected towards MM1.

5 CONCLUSION

In this article, we present the identification of the emission lines of HNCO and NH_2CHO towards hot core MM1 using the ALMA bands 6 and 7. The conclusions of this study are summarised below:

1. We successfully detected four and six non-blended rotational transition lines of peptide bond molecules NH_2CHO and HNCO towards the hot core MM1.
2. The estimated column densities of NH_2CHO and HNCO towards the MM1 are $(2.80 \pm 0.29) \times 10^{15} \text{ cm}^{-2}$ and $(1.80 \pm 0.42) \times 10^{16} \text{ cm}^{-2}$ with excitation temperatures of $165 \pm 21 \text{ K}$ and $170 \pm 32 \text{ K}$, respectively. The fractional abundances of NH_2CHO and HNCO towards the MM1 are $(9.03 \pm 1.44) \times 10^{-10}$ and $(5.80 \pm 2.09) \times 10^{-9}$.
3. We compared the estimated abundances of NH_2CHO and HNCO with the existing three-phase warm-up chemical model abundances and noticed that the observed and modelled abundances are very close.
4. We claim that NH_2CHO is produced by the reaction of NH_2 and H_2CO in the gas phase towards MM1. Similarly, HNCO is created by the reaction of NH and CO on the grain surface of MM1.
5. We also discuss the chemical links between NH_2CHO and HNCO . According to the correlation equation of [López-Sepulcre et al. \(2015\)](#), both NH_2CHO and HNCO are chemically linked towards the MM1. The presence of NH_2CHO and HNCO indicates that other O- and N-bearing molecules exist in this source, which we discuss in follow-up studies.

ACKNOWLEDGMENTS

We thank the anonymous referee for the helpful comments that improved the manuscript. A.M. acknowledges the SVMCM for financial support for this research. This paper makes use of the following ALMA data: ADS /JAO.ALMA#2019.1.00768.S and ADS /JAO.ALMA#2018.A.00031.T. ALMA is a partnership of ESO (representing its member states), NSF (USA), and NINS (Japan), together with NRC (Canada), MOST and ASIAA (Taiwan), and KASI (Republic of Korea), in co-operation with the Republic of Chile. The joint ALMA Observatory is operated by ESO, AUI/NRAO, and NAOJ.

CONFLICTS OF INTEREST

The authors declare no conflict of interest.

References

- Adande, G. R., Woolf, N. J., & Ziurys, L. M. 2013, *Astrobiol.*, 13, 439
- Adande, G. R., Halfen, D. T., Ziurys, L. M., Quan, D., Herbst, E. 2010, *ApJ*, 725, 561

- Bisschop, S. E., Jørgensen, J. K., van Dishoeck, E. F. et al. 2007, *A&A*, 465, 913
- Belloche, A., Müller, H. S. P., Menten, K. M. et al. 2013, *A&A*, 559, A47
- Beuther, H., Churchwell, E. B., McKee, C. F., Tan, J. C., 2007, in Reipurth B., Jewitt D., Keil K.eds, *Protostars and Planets V*. University of Arizona Press, Tucson, AZ, p. 165
- Bisschop, S. E., Jørgensen, J. K., van Dishoeck, E. F., & de Wachter, E. B. M. 2007, *A&A*, 465, 913
- Bisschop, S. E., Jørgensen, J. K., Bourke, T. L., Bottinelli, S., & van Dishoeck, E. F. 2008, *A&A*, 488, 959
- Brogan, C. L., Hunter, T. R., Towner, A. P. M., et al. 2019, *ApJL*, 881, L39
- Bayandina, O.S., Brogan, C.L., Burns, R.A., et al. 2022, *AJ*, 163(2), p.83
- Bockelée-Morvan, D., Lis, D. C., Wink, J. E., et al. 2000, *A&A*, 353, 1101
- Biver, N., Bockelée-Morvan, D., Debout, V., et al. 2014, *A&A*, 566, L5
- Colzi, L., Rivilla, V. M., Beltrán, M. T., et al., 2021, *A&A*, 653, A129
- Codella, C., Ceccarelli, C., Caselli, P., et al. 2017, *A&A*, 605, L3
- Chen, X., Sobolev, A. M., Ren, Z.-Y., et al. 2020, *NatAs*, 4, 1170
- Churchwell, E., Wood, D., Myers, P. C., & Myers, R. V. 1986, *ApJ*, 305, 405
- Coutens, A., Jørgensen, J. K., van der Wiel, M. H. D., et al., 2016, *A&A*, 590, L6
- Blake, G. A., Sutton, E. C., Masson, C. R., & Phillips, T. G. 1987, *ApJ*, 315, 621
- Canelo, C. M., Bronfman, L., Mendoza, E., et al., 2021, *MNRAS*, 504, 4428
- Fedoseev G., Ioppolo S., Zhao D., Lamberts T., Linnartz H., 2015, *MNRAS*, 446, 439
- Goemann, F., Rosenbauer, H., Bredehöft, J. H., et al. 2015, *Science*, 349, 020689
- Gorai P., Bhat B., Sil M., Mondal S. K. Ghosh R., Chakrabarti S. K., Das A., 2020, *ApJ*, 895, 86
- Garrod R. T., Weaver S. L. W., Herbst E., 2008, *ApJ*, 682, 283
- Garrod, R. T. 2013, *ApJ*, 765, 60
- Herbst E., & van Dishoeck E. F., 2009, *ARA&A*, 47, 427
- Halfen, D. T., Ilyushin, V., Ziurys, L. M. 2011, *ApJ*, 743, 60
- Haupa, K. A., Tarczay, G., & Lee, Y.-P. 2019, *JChS*, 141, 11614
- Hernández-Gómez, A., Sahnoun, E., Caux, E., et al., 2019, *MNRAS*, 483, 2014
- Iglesias E., 1977, *ApJ*, 218, 697
- Jackson, J. M., Armstrong, J. T., & Barrett, A. H. 1984, *ApJ*, 280, 608
- Kurland, R. J., & Wilson, E. B., 1957, *J. Chem. Phys.* 27, 585
- Kahane, C., Ceccarelli, C., Faure, A., & Caux, E. 2013, *ApJ*, 763, L38
- Kukulich, S. G., Nelson, A. C., Yamanashi, B. S., 1971, *J. Am. Chem. Soc.* 93(25), 6769-6771
- Kuan, Y., & Snyder, L. E. 1996, *ApJ*, 470, 981
- López-Sepulcre, A., Jaber, A. A., Mendoza, E., et al. 2015, *MNRAS*, 449, 2438
- Lapinov A. V., Golubiatnikov G. Y., Markov V. N., Guarnieri A., 2007, *Astron. Lett.*, 33, 121

- Ligterink N. F. W., Terwisscha van Scheltinga J., Taquet V., Jørgensen J. K., Cazaux S., van Dishoeck E. F., Linnartz H., 2018, *MNRAS*, 480, 3628
- Mendoza, E., Lefloch, B., López-Sepulcre, A., et al. 2014, *MNRAS*, 445, 151–353, 1101
- Muller, S., Beelen, A., Black, J. H., et al. 2013, *A&A*, 551, A109
- MacDonald, G. H., Gibb, A. G., Habing, R. J., & Millar, T. J. 1996, *A&AS*, 119, 333
- Manna, A., Pal, S., 2022a, *Life Sciences in Space Research*, 34, 9
- Manna, A., Pal, S., 2022b, *Journal of Astrophysics and Astronomy*, 43, 83
- Manna, A., & Pal, S., 2023, *Astrophys Space Sci*, 368, 33
- Manna, A., Pal, S., Viti, S., Sinha, S., 2023, *MNRAS*, 525, 2229–2240
- Manna, A., Pal, S., Baug, T., Mondal, S., 2024, *Res. Astron. Astrophys*, 24, 065008
- Manna, A., Pal, S., Viti, S., 2024, submitted in *MNRAS*
- Manna, A., & Pal, S., 2024, *New Astronomy*, 109, 102199
- McMullin, J. P., Waters, B., Schiebel, D., Young, W., Golap, K. 2007. *CASA Architecture and Applications*. Astronomical Society of the Pacific Conference Series, Vol. 376, *Astronomical Data Analysis Software and Systems XVI*, ed. R. A. Shaw, F. Hill, & D. J. Bell, 127
- Müller, H. S. P., Schlmöder, F., Stutzki, J. Winnewisser, G., 2005, [Journal of Molecular Structure](#), 742, 215
- Niedenhoff M., Yamada K. M. T., Belov S. P., Winnewisser G., 1995, *Journal of Molecular Spectroscopy*, 174, 151
- Perley, R. A., Butler, B. J. 2017, *ApJ*, 230, 1538
- Pickett, H. M., Poynte, R. L., Cohen, E. A., et al. 1998, *Journal of Quantitative Spectroscopy and Radiative Transfer*, 60, 883
- Quan D., Herbst E., 2007, *A&A*, 474, 521
- Rubin R. H., Swenson G. W., Jr, Benson R. C., Tigelaar H. L., Flygare W. H., 1971, *ApJ*, 169, L39
- Reid, M. J., Menten, K. M., Brunthaler, A., et al. 2014, *ApJ*, 783, 130
- Redondo P., Barrientos C., Largo A., 2014, *ApJ*, 780, 181
- Saladino, R., Crestini, C., Pino, S., Costanzo, G., & Di Mauro, E. 2012, *Physics of Life Reviews*, 9, 84
- Snyder, L. E., & Buhl, D. 1972, *ApJ*, 177, 619
- Stecklum, B., Wolf, V., Linz, H., et al., 2021. *A&A*, 646, p.A161
- Turner, B. E., Terzieva, R., & Herbst, E. 1999, *ApJ*, 518, 699
- Turner B. E., 2000, *ApJ*, 542, 837
- Tercero, B., Cernicharo, J., Pardo, J. R., Goicoechea, J. R. 2010, *A&A*, 517, A96
- van Dishoeck E. F. & Blake G. A., 1998, *Annu Rev Astron Astrophys*, 36, 317
- van Dishoeck, E. F., Blake, G. A., Jansen, D. J., & Groesbeck, T. D. 1995, *ApJ*, 447, 760

- Vastel, C., Bottinelli, S., Caux, E., Glorian, J. -M., Boiziot, M., 2015, CASSIS: a tool to visualize and analyse instrumental and synthetic spectra. Proceedings of the Annual meeting of the French Society of Astronomy and Astrophysics, 313-316
- Williams D. A., Viti S., 2014, Observational Molecular Astronomy: Exploring the Universe Using Molecular Line Emissions. Cambridge Univ. Press, Cambridge
- Yamaguchi, T., Takano, S., Watanabe, Y., et al. 2012, PASJ, 64, 105
- Zinchenko, I., Henkel, C., & Mao, R. Q. 2000, A&A, 361, 1079